

Corrosion Behavior of Al-3.0 wt.%Mg Alloy by Cold-Drawing Process

Xin Zhang^{1,2}, Zehua Wang^{1,*}, Zehua Zhou¹, Jing Cao¹, Guangheng Yang¹

¹ College of Mechanics and Materials, Hohai University, Nanjing, 210098, China

² Nantong Ocean and Offshore Engineering Research Institute, Hohai University, Nantong, 226300, China

*E-mail: zhangxin.007@163.com

Received: 1 October 2019 / Accepted: 2 December 2019 / Published: 31 December 2019

In this study, the evolution of cold-drawn corrosion behavior of Al-3.0 wt.%Mg alloy was investigated by microstructure observation, immersion test and electrochemical measurement. Results indicated that, during the cold drawing process, the equiaxial grains of alloy were elongated and pressed into fibrous and globular grains on longitudinal section (I) and cross section (II), respectively. Meanwhile, the large size skeletal FeAl₃ phase particles were elongated and fragmented into small size lining particles on I section, and pressed into small globular particles on II section. As the strain increased, the corrosion resistance increased and the pitting sensibility decreased, while the corrosion sensibility increased first and then decreased. Finally, compared to the alloy on longitudinal section, the alloy on cross section revealed better corrosion resistance and lower pitting sensibility.

Keywords: cold-drawing process Al-3.0 wt.%Mg alloy, corrosion behavior, pitting corrosion.

1. INTRODUCTION

As a functional material with excellent corrosion resistance, high mechanical property and low electric resistivity, Al-Mg alloy wires have been widely used in electromagnetic shielding materials [1-3]. Nowadays, alloy wires are usually prepared by continuous casting. The diameters of the cast alloy wires, however, are too large to produce the electromagnetic shielding net. Therefore, a cold-drawing process is needed to obtain fine wires for electromagnetic shielding net woven.

It is well-known that severe plastic deformation would refine the microstructure and enhance the mechanical property of metals [4-6]. However, the effects of plastic deformation on corrosion behavior of metals are complex [7-14]. For example, inconsistent results were often obtained when same deformation processing was applied to different aluminum alloys. In general, equal channel angular

pressing (ECAP) would reduce the corrosion resistance of commercial aluminum alloy due to the decomposition of Fe-rich phase particles that increase the pitting sensitivity and dissolution of the aluminum matrix [7,8]. However, ECAP could also refine α -Al crystal where pit initiation and growth occur preferentially, while reducing the weakness of the depletion zone around the second phase precipitates, thus improving the corrosion resistance of Al-5.4Ni, Al-5%Cu and AA 2024 alloys [8,9].

The microstructure and mechanical properties evolutions of Al-3.0 wt.%Mg alloy wire, as well as the relationship between them during cold drawing processing, have been investigated in previous study [15]. Result showed that, as the strain increased, the grains of the alloys were elongated and the second phase particles were fragmented, resulting in the linear increase of the strength and three-stage decline of the plasticity. However, the corrosion behavior of cold-drawn Al-3.0 wt.%Mg alloy wires with different strains remains unknown, and the relationship between cold-drawn strain and corrosion resistance needs to be investigated. With this in mind, this study aimed to study the evolution of microstructure and corrosion behavior of Al-3.0 wt.%Mg alloy in cold-drawing processing. In particular, the effect of cold-drawn strain on the corrosion resistance of Al-3.0wt.%Mg alloy wires with different sections was investigated.

2. EXPERIMENTAL

2.1 Material preparation

Al-3.0 wt.%Mg alloy was prepared from pure aluminum ingot (99.7 wt,%) and pure magnesium ingot (99.9 wt.%) in an electrical resistance furnace at a melting temperature of 720 °C. The degassing process was conducted with argon before pouring. The metal mould was used for pouring to obtain a dense test bar which was then machined to Φ 10 mm. The chemistry of Al-3.0 wt%Mg alloy is summarized and shown in Table 1.

Table 1. The composition of Al-3.0 wt%Mg alloy (wt%)

Element	Mg	Fe	Si	Al
wt.%	2.97	0.14	0.09	<i>Bal.</i>

2.2 Cold-drawing process

Wire drawing machine was used to manufacture the Al-3.0 wt.%Mg alloy wire from Φ 10 mm to Φ 2 mm by 15 passes, as shown in Fig.1. The diameter of the alloy wire after each drawing pass was listed in Table 2. The microstructure and corrosion behavior of Al-3.0 wt.%Mg alloy wires with diameters of 7, 6, 5, 4, 3 and 2 mm were tested.

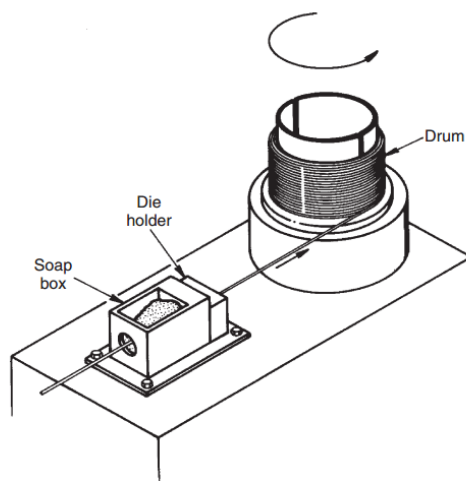


Figure 1. Diagrammatic sketch of wire drawing machine

Table 2. Diameter and strain of Al-Mg alloy wire of each drawing pass

Pass	1	2	3	4	5	6	7	8	9	10	11	12	13	14	15
Diameter (mm)	9.0	8.0	7.0	6.0	5.0	4.5	4.0	3.8	3.5	3.2	3.0	2.8	2.5	2.2	2.0
Strain (%)	19.0	36.0	51.0	64.0	75.0	79.8	84.0	85.6	87.8	89.8	91.0	92.2	93.8	95.2	96.0

2.3 Microstructure analysis

Microstructures of the alloy wires with different cold drawing strains were evaluated before and after immersion test using Olympus-BX51M optical microscopy (OM) and Hitachi S-3400N scanning electron microscopy. Longitudinal section (I) and cross section (II) of Al-3.0 wt.%Mg alloy wires with different strains were prepared for the microstructure analysis and corrosion test, as shown in Fig.2.

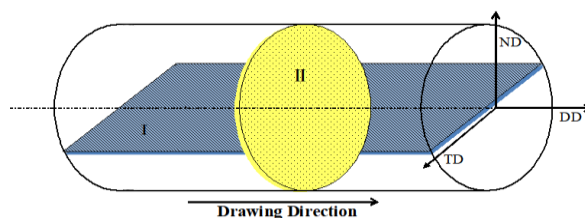


Figure 2. Diagrammatic sketch of sample option for structure analysis and corrosion test: Longitudinal section (I); Cross section (II).

2.4 Immersion test and electrochemical measurement

The corrosion test was applied to the longitudinal section (I) and cross section (II) of the Al-3.0 wt.%Mg alloy wires with different strains (Fig.2). In addition, the immersion test and electrochemical measurement were conducted in a unsaturated 3.5 wt.%NaCl solution, after which the specimens were

kept in NaCl solution for 120 hours. The electrochemical measurement was conducted using the PARSTAT 2273 electrochemical workstation, which used a three-electrode system including working electrode (specimen), reference electrode (232 model saturated calomel electrode) and auxiliary electrode (213 model Pt wire). After open circuit potential was stable, electrochemical impedance spectroscopy (EIS) and potentiodynamic polarization were tested according to ASTM G3-13[16]. In particular, EIS test was conducted in the frequency from 10^5 to 10^{-2} Hz, while the scanning rate of potentiodynamic polarization experiment was 0.1 mV/s. All measurements were repeated at least three times to ensure the accuracy of the results.

3. RESULTS AND DISCUSSION

Fig.3 shows the microstructure and EDS analysis result of as-cast Al-3.0 wt.% alloy. Specifically, the grains in as-cast Al-3.0 wt.%Mg alloy were equiaxial crystal, wherein apparent developed dendrite was observed. The 3D morphology of second phase, obtained by deep etch, showed that particles were skeletal in shape and were mainly dispersed at the grain boundaries (Fig.3 (c)). EDS analysis indicated that the skeletal particles consisted of elements of Al, Mg and Fe. According to previous studies [17,18], the skeletal particles observed in our study should be $FeAl_3$ phase.

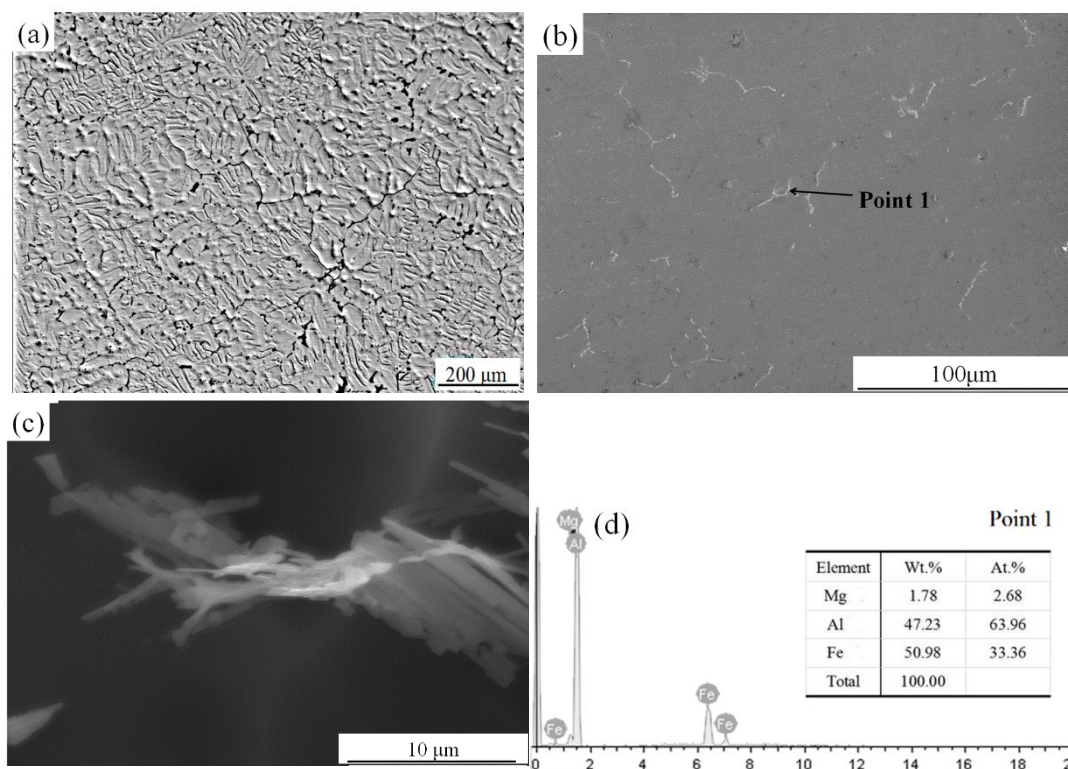


Figure 3. Microstructure and EDS results of Al-3.0 wt.%Mg alloy: (a) optical image; (b) SEM image; (c) 3D morphology of second phase; (d) EDS result

The microstructures of Al-3.0 wt.%Mg alloy wires with different strains on I section and II section are shown in Fig.4. On I section, the equiaxial grains were gradually elongated into fibrous

crystals, and grain boundaries were aligned into a lamellar structure along the drawing direction during the cold-drawing process. On \perp section, the equiaxial grains were suppressed, grain size was reduced, and grain boundary density was increased. In addition, the grain diameter decreased from 271 μm to 12 μm while the strain increased from 0% to 96%. In general, the grains in Al-3.0 wt.%Mg alloy wire changed from equiaxial shape to fiber shape along the cold drawing direction during the processing.

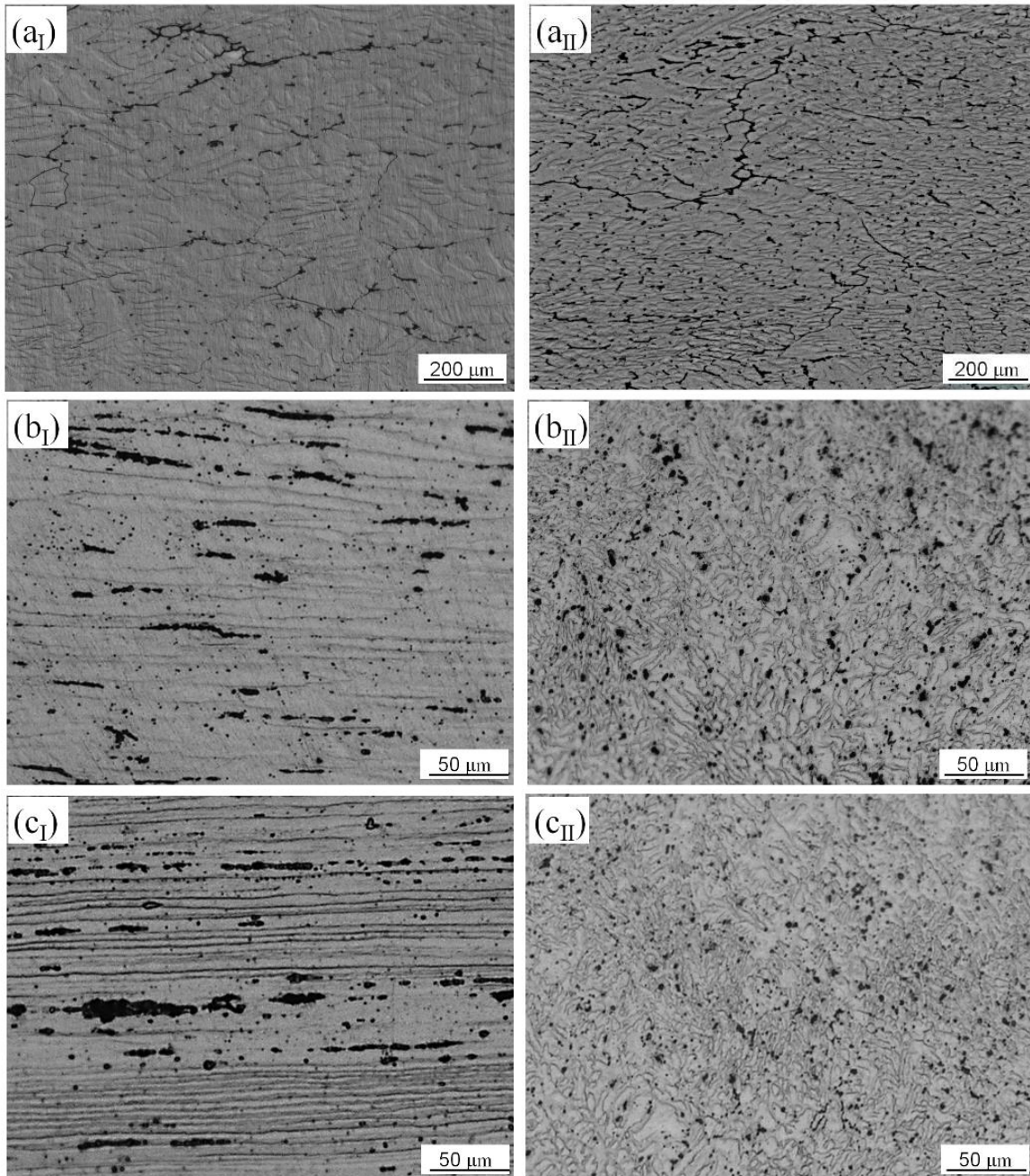


Figure 4. Optical micrograph on \perp and \parallel sections of Al-3.0 wt.%Mg alloy wires with different strains: (a) 51%, (b) 84%, (c) 96%

Fig.5 shows the shape and distribution of the second phase particles of Al-3.0 wt.%Mg alloy

wires with different strains on I and II section. Specifically, during the cold drawing process, the second phase particles were fragmented. When the strain was 51%, the skeletal FeAl_3 phase particles were elongated on I section and compressed on II section. However, the deformation extent of the particles was mild, suggesting that the distinction between the phase particles on I section and II section was not obvious. When the strain was 84%, the skeletal phase particles were elongated to finer globular particles and arranged in lines on I section, while the skeletal particles disappeared and were replaced by finer globular particles on II section.

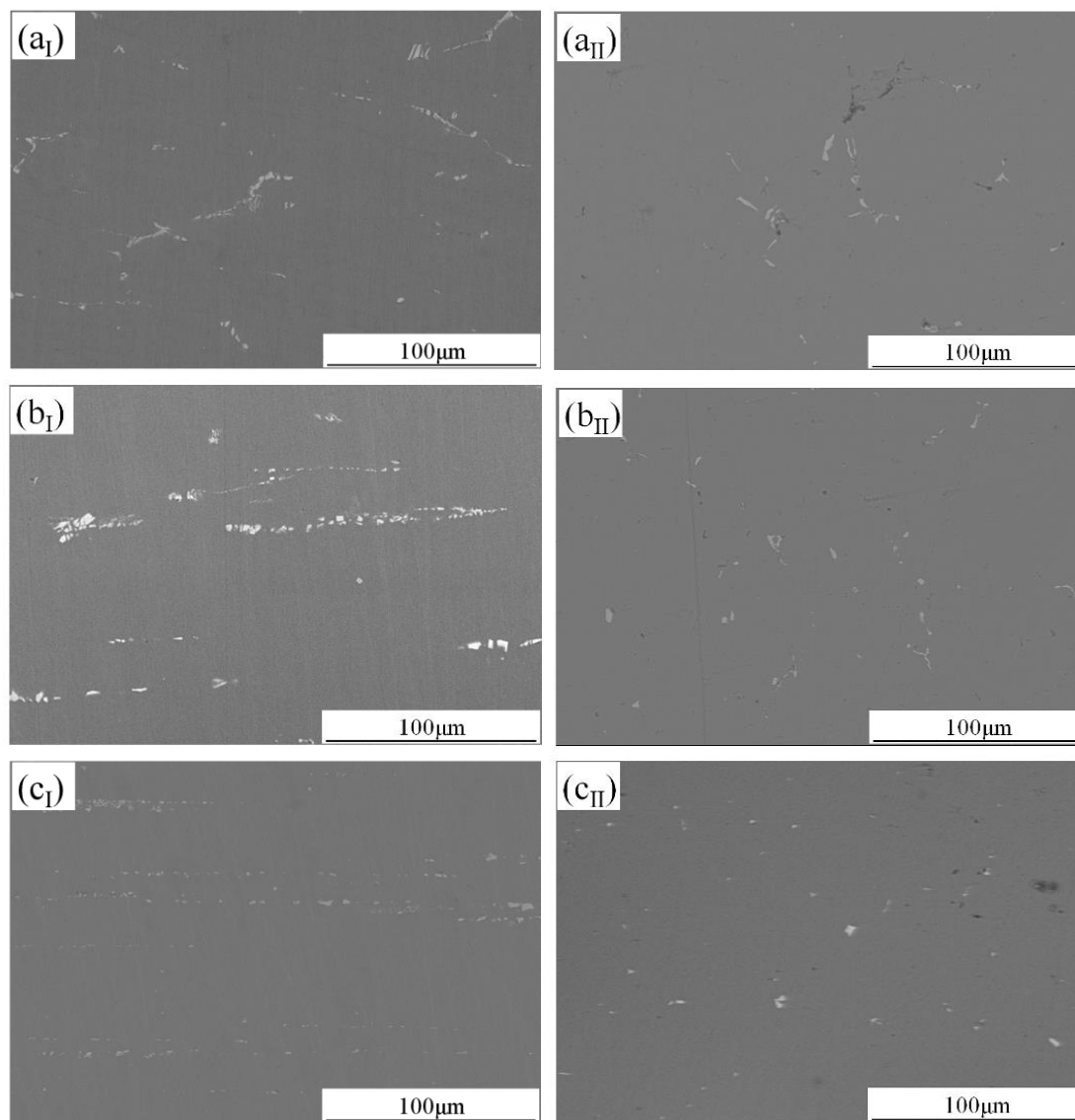


Figure 5. Second phase particles shape and distribution on I and II sections of Al-3.0 wt.%Mg alloy wires with different strains: (a) 51%; (b) 84%; (c) 96%.

When the strain was 96%, the globular phase particles became smaller and the linearly distributed particles became longer on I section, while on II section the globular particles became smaller. In

general, the skeletal form of $FeAl_3$ phase particles on I section was gradually decomposed into finer globular particles and arranged in lines along the drawing direction, while the particles on II section were pressed into globular shape with smaller size. Fig.6 shows the surface morphology of the as-cast Al-3.0 wt.%Mg alloy after immersion in 3.5 wt.% NaCl solution for 120 hours. It can be seen that a large number of pitting holes around $FeAl_3$ phase particles appeared on the surface of the immersed alloy in a form of islands (Fig.6 (b)).

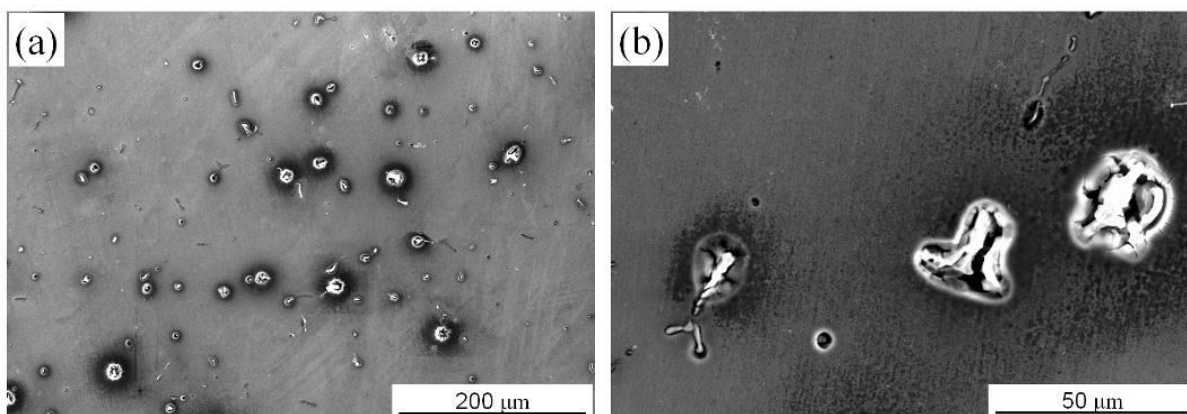
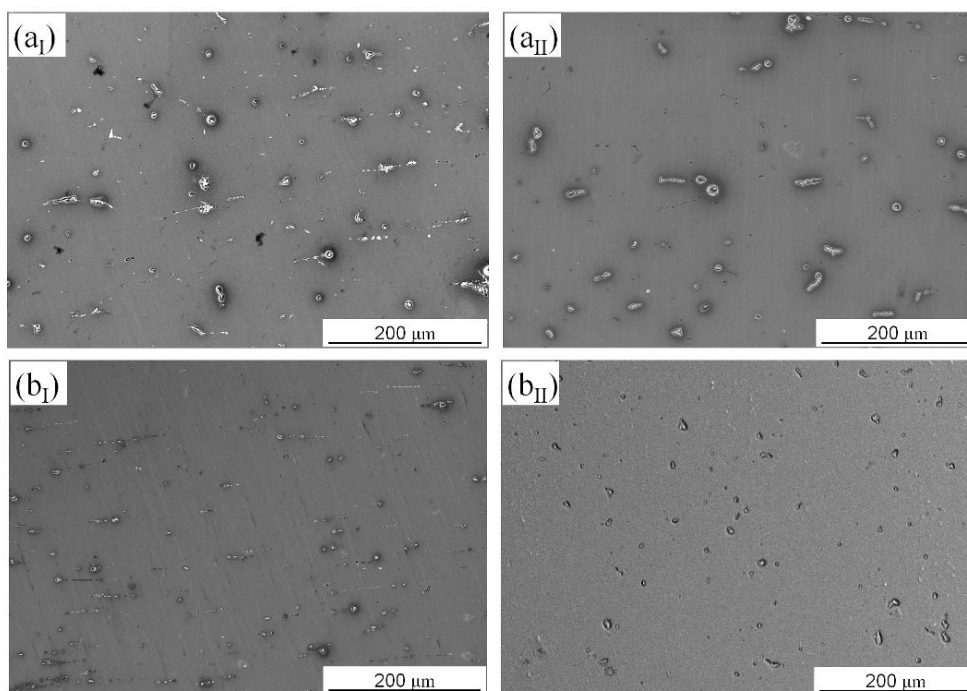


Figure 6. Surface morphology of Al-3.0 wt.%Mg alloy corroded in 3.5 wt.% NaCl for 120 hours.

Surface morphologies of Al-3.0wt.%Mg alloys with different strains corroded in NaCl solution on I and II sections are shown in Fig.7, wherein the pitting corrosion occurred around the fragmented $FeAl_3$ phase particles.



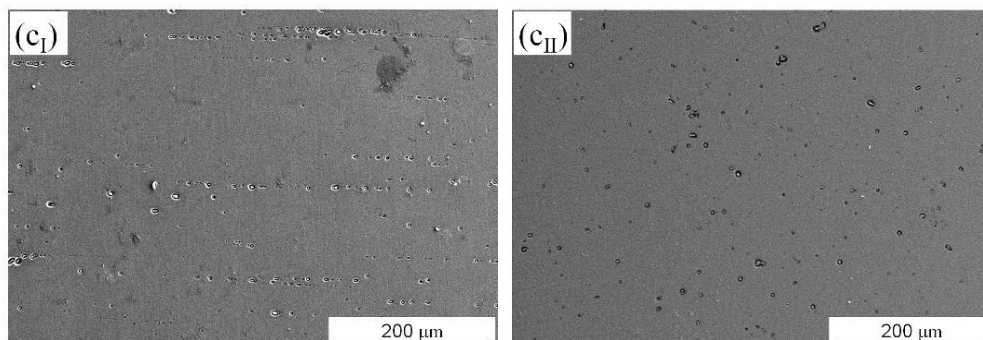


Figure 7. Surface morphologies on I and II sections of Al-3.0wt.%Mg alloys with different strains corroded in 3.5 wt.% NaCl solution for 120 hours: (a) 0%, (b) 51%, (e) 84%, (g) 96%.

Specifically, as the strain increased, the amount of corrosion pitting holes increased and the diameter of the pitting holes decreased in the unit area on both I and II sections. The amount of the pitting holes on I section, however, was significantly higher than that of the alloy wire with the same cold drawing strain on II section.

Fig.8 shows the potentiodynamic polarization curves of Al-3.0 wt.%Mg alloys with different strains on I and II sections.

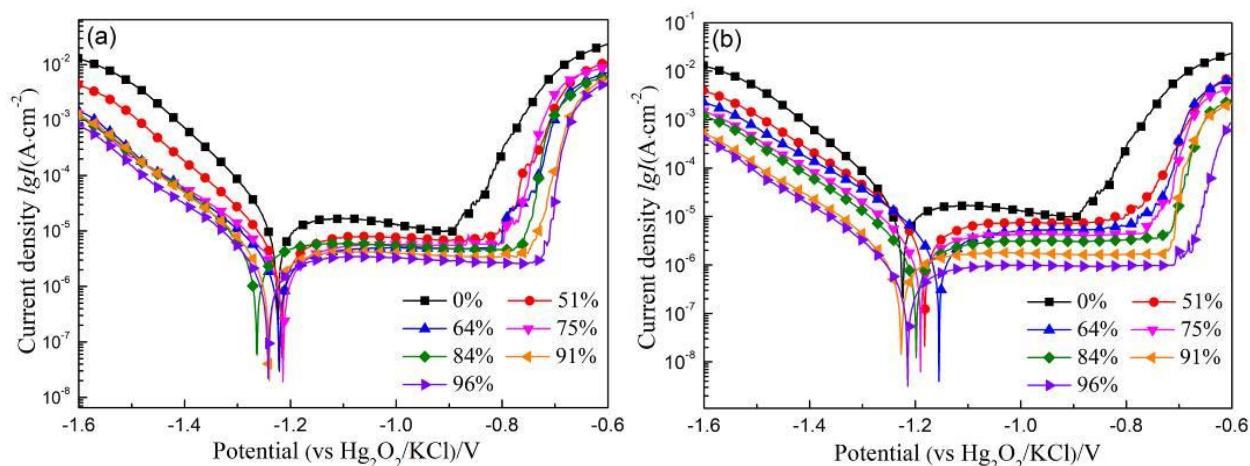


Figure 8. Potentiodynamic polarization curves of Al-3.0 wt.%Mg alloys with different strains: (a) I section, (b) II section

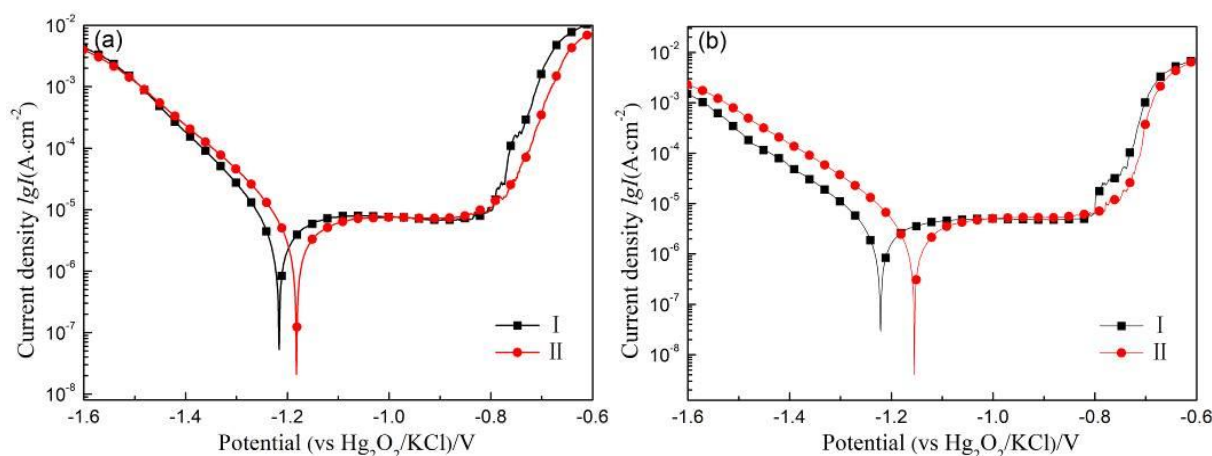
A passive area with constant current was observed in the anodic branch of the polarization curve, and there was no Tafel region in the anodic polarization. The Cathode extrapolation was then applied to the Tafel curves and the corrosion potential (E_{corr}) to calculate the corrosion current density (i_{corr}) and the pitting corrosion potential (E_{pit}) (Table 3). It can be observed that, as the strain increased, i_{corr} value decreased and E_{pit} value increased subsequently, while E_{corr} value increased first and then decreased. On

I section, the alloy wire with 51% strain revealed the highest E_{corr} , while the alloy wire with 64% strain had the highest E_{corr} on II section. Additionally, result also suggested that the cold drawing processing could increase the corrosion resistance and decrease the pitting sensibility of Al-3.0 wt.%Mg alloy. That is, the higher cold drawing strain, the better corrosion resistance and lower pitting sensibility of alloy wire.

Table 3. E_{corr} , i_{corr} , E_{pit} values of Al-3.0 wt.%Mg alloy derived from the polarization curves.

Strain	E_{corr}/V		$E_{corr-II} - E_{corr-I}$	$i_{corr}/\mu A \cdot cm^{-2}$		$i_{corr-II} - i_{corr-I}$	E_{pit}/V		$E_{pit-II} - E_{pit-I}$
	I section	II section		I section	II section		I section	II section	
0%	-1.228			7.57			-0.924		
51%	-1.217	-1.176	0.041	5.361	5.289	-0.072	-0.821	-0.818	0.003
64%	-1.222	-1.154	0.068	4.212	3.932	-0.980	-0.803	-0.789	0.014
75%	-1.223	-1.188	0.035	3.701	3.078	-0.623	-0.795	-0.763	0.032
84%	-1.263	-1.198	0.065	3.443	2.071	-1.372	-0.765	-0.731	0.034
91%	-1.238	-1.226	0.012	2.679	1.181	-1.498	-0.751	-0.725	0.026
96%	-1.240	-1.213	0.027	2.511	0.672	-1.839	-0.725	-0.712	0.013

Fig.9 presents the comparison of potentiodynamic polarization curves of Al-3.0 wt.%Mg alloys with different cold drawing strains on I and II sections. Interestingly, E_{corr} value and E_{pit} value on I section were lower than those of the alloy wires with the same strain on II section. The i_{corr} value on I section was higher than that on II section.



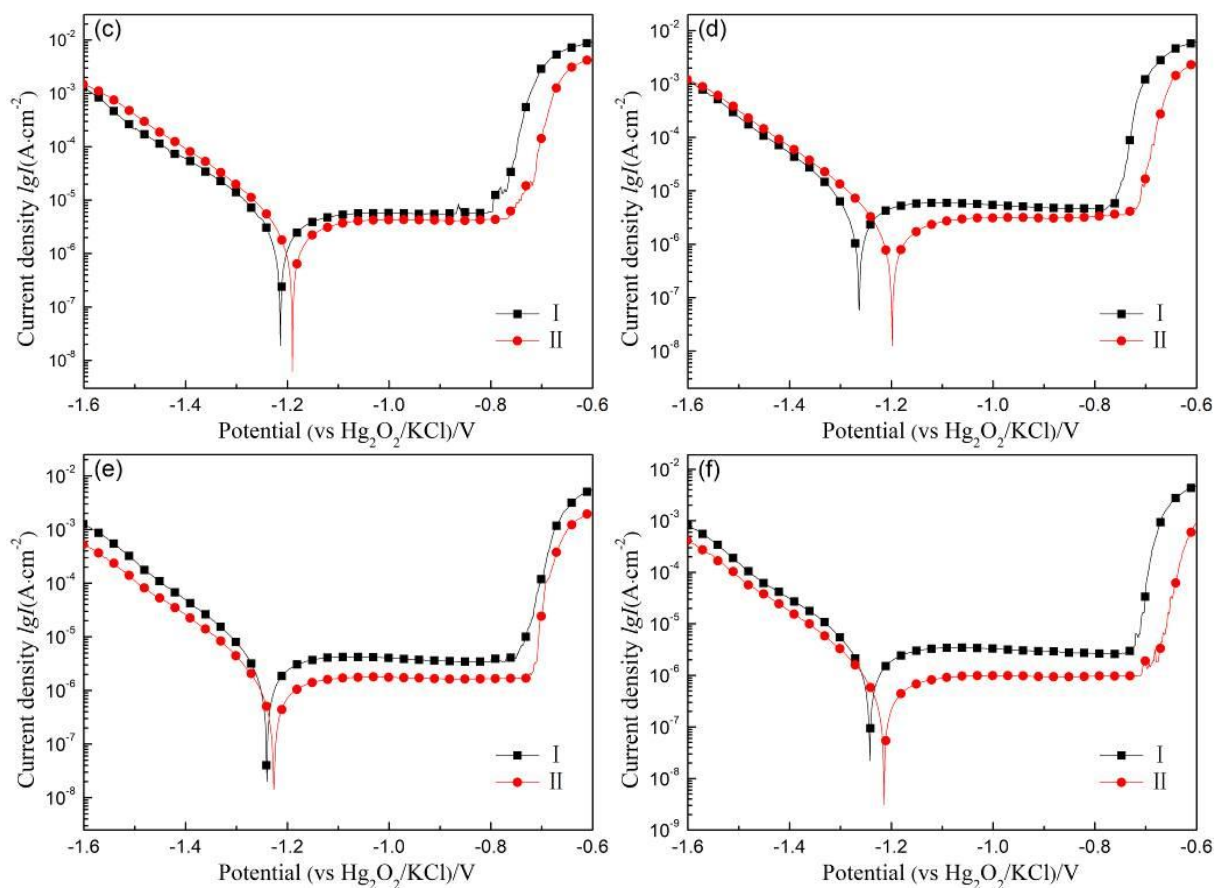


Figure 9. The difference between potentiodynamic polarization curves on I and II sections of Al-3.0 wt.%Mg alloys with the same strain: (a) 51%, (b) 64%, (c) 75%, (d) 84%, (e) 91%, (f) 96%.

This finding indicated that cold-drawn Al-3.0 wt.%Mg alloy on cross section (II section) yielded better corrosion resistance, lower corrosion and pitting sensibility compared to the alloy on longitudinal section (I section) under the same cold drawing strain. Furthermore, the difference of i_{corr} and E_{pit} between II and I section ($i_{corr-II} - i_{corr-I}$ and $E_{pit-II} - E_{pit-I}$) tended to increase as the the strain increased, demonstrating that the difference of corrosion resistance and pitting sensibility between I and II sections increased accordingly during the cold drawing processing.

The Nyquist diagram of Al-3.0 wt.%Mg alloys with different strains on I and II sections was shown in Fig.10. Two capacitive impedance arcs could be seen in Nyquist diagram. In general, high frequency capacitive loop is attributed to the charge transfer reaction in the electric double layer formed at the corrosive medium close to the metal specimens, which can be defined by the charge transfer resistance (R_t) and the oxide-layer capacitance of the original flat surface (Q_p) [19-21]. Low frequency capacitive loop, which can be defined by $Q_{dl(pit)}$ and $R_{t(pit)}$, is usually associated with the mass transport in the solid phase and diffusion of ions through the oxide films or the stable passive films on the surface. Therefore, EIS of the tested alloys can be represented by an equivalent circuit of Fig.11. In this study, the parameters of the equivalent circuit were calculated by ZSimpWin software and the results were summarized in Table 4. In general, the diameter of the capacitive circle is associated with the charge

transfer resistance. The larger the diameter of the capacitor circle, the slower the corrosion rate and the better the corrosion resistance. In this study, the R_t denotes the activity of the alloys and the $R_{t(pit)}$ denotes the resistance of ion diffusion through the passive films. The higher the values of R_t and $R_{t(pit)}$, the lower the activity of the alloys and the more stable and dense the passive films. As the cold drawing strain increased, the diameter of the capacitive circle, R_t and $R_{t(pit)}$, increased rapidly first and then slowed down on I section, while the capacitive circle diameter, R_t and $R_{t(pit)}$, increased sustainably on II section. This finding indicates that the cold drawing processing could improve the corrosion resistance of Al-3.0 wt.%Mg alloy. Specifically, On I section, the cold drawing process improved the corrosion resistance greatly when the strain was 51%, and this improvement tended to slow down when the strain was over 51%. On II sections, however, the corrosion resistance of the alloy wire increased drastically with the increasing strain.

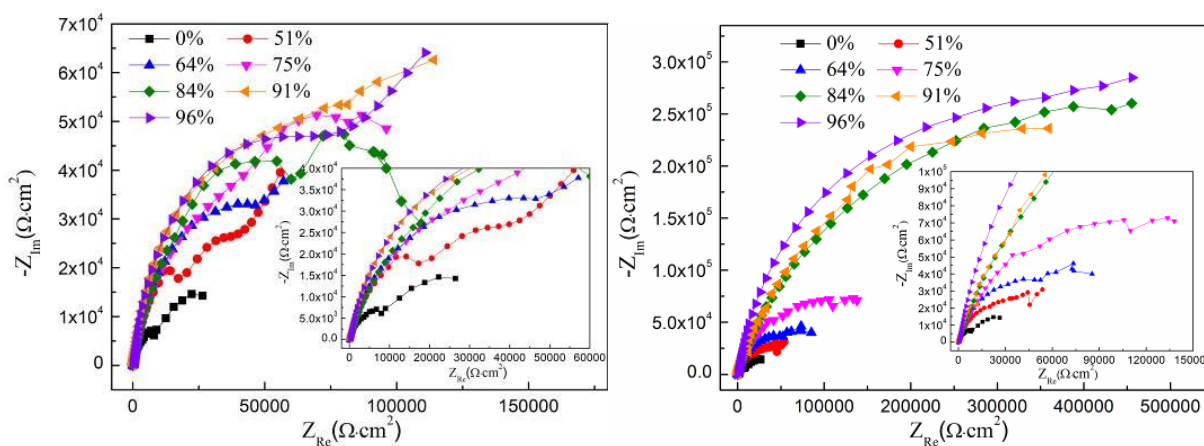


Figure 10. Nyquist diagram of Al-3.0 wt.%Mg alloys with different strains: (a) I section, (b) II section

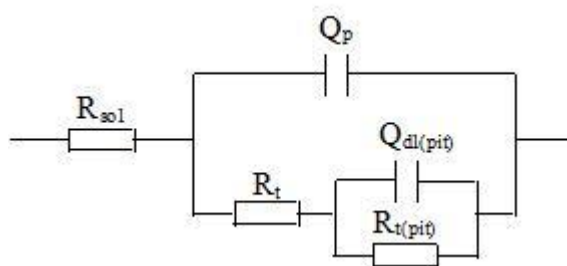


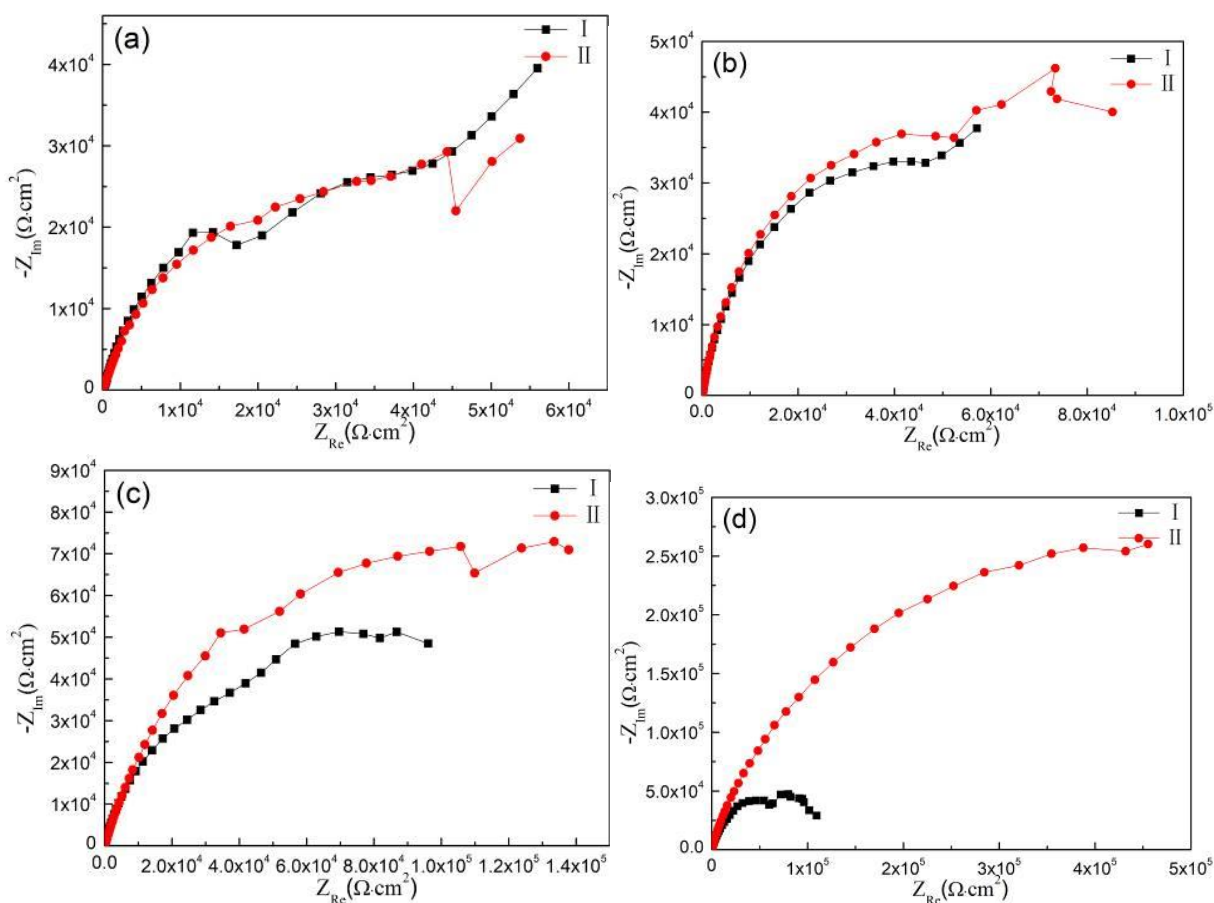
Figure 11. An equivalent circuit for the tested alloys

Table 4. The parameters of the equivalent elements in equivalent circuit for different alloys.

Strain (%)	Section	R_{sol} ($\Omega \cdot \text{cm}^2$)	Q_p ($\Omega^{-1} \cdot \text{cm}^{-2} \cdot \text{s}^{-1}$)	n1	R_t ($\Omega \cdot \text{cm}^2$)	Q_{dl} ($\Omega^{-1} \cdot \text{cm}^{-2} \cdot \text{s}^{-1}$)	n2	$R_{t(pit)}$ ($\Omega \cdot \text{cm}^2$)
0		9.53	9.02×10^{-6}	0.8771	1.78×10^4	10.04×10^{-6}	0.9432	1.28×10^4
51	I	24.27	5.98×10^{-6}	0.7726	8.10×10^4	5.10×10^{-6}	0.9829	5.56×10^4
	II	4.25	6.36×10^{-6}	0.9433	8.33×10^4	6.47×10^{-6}	0.8985	5.49×10^4

64	I	18.60	3.07×10^{-6}	0.8136	8.33×10^4	5.81×10^{-6}	0.9539	8.57×10^4
	II	3.48	5.46×10^{-6}	0.8230	9.63×10^4	5.53×10^{-6}	0.8736	9.22×10^4
75	I	13.42	4.71×10^{-6}	0.8177	10.03×10^4	20.27×10^{-6}	0.9450	6.81×10^4
	II	2.13	6.75×10^{-6}	0.8999	20.23×10^4	4.22×10^{-6}	0.8784	12.31×10^4
84	I	19.51	2.64×10^{-6}	0.7758	13.34×10^4	9.81×10^{-6}	0.8361	8.06×10^4
	II	1.17	14.21×10^{-6}	0.9168	25.04×10^4	5.03×10^{-6}	0.7922	36.62×10^4
91	I	14.30	4.84×10^{-6}	0.8512	12.89×10^4	5.73×10^{-6}	0.8539	20.52×10^4
	II	1.15	5.11×10^{-6}	0.8958	33.70×10^4	4.70×10^{-6}	0.9861	73.01×10^4
96	I	23.67	2.76×10^{-6}	0.8448	12.87×10^4	3.34×10^{-6}	0.9289	22.14×10^4
	II	1.12	3.02×10^{-6}	0.9887	42.58×10^4	6.45×10^{-6}	0.9374	80.23×10^4

Fig.12 shows the comparison of Nyquist diagram of Al-3.0 wt.%Mg alloys with different strains on I and II sections. The difference between the capacitive circle diameter, R_t and $R_{t(pit)}$, on I and II sections was small when the strain was 51%. In contrast, when the strain exceed 51%, this difference gradually increased as the strain increased. This finding implies that the corrosion resistance on II section was better than that on I section, and the difference of corrosion resistance between I and II sections increased with the increasing cold drawing strain.



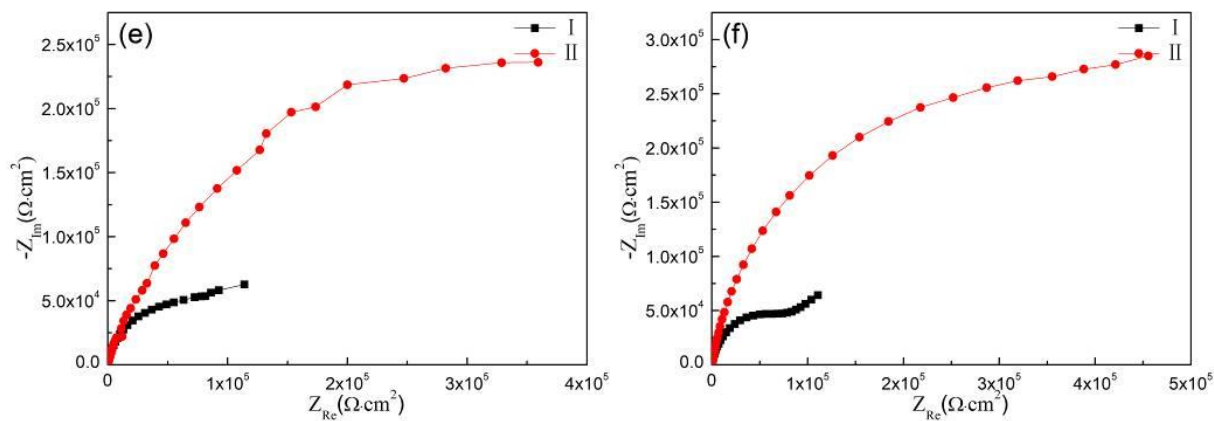


Figure 12. Comparison of Nyquist diagram on I and II sections of Al-3.0 wt.%Mg alloys with the same strain: (a) 51%, (b) 64%, (c) 75%, (d) 84%, (e) 91%, (f) 96%.

The corrosion behavior of Al-3.0 wt.%Mg alloy wires varied with the microstructure evolution during cold drawing process. Plastic deformation could refine the grains and cause dislocations and grain boundaries, leading to changes in the corrosion resistance of the aluminum alloys [7-9]. However, the influence of second phase on corrosion behavior of the alloys should not be neglected. As we mentioned before, pitting corrosion occurred around FeAl_3 phase particles. The exist of FeAl_3 phases destroys the continuity of Al-3.0 wt.%Mg alloy. FeAl_3 phases have much higher electrode potential (0.56 V) than Al matrix (about 0.85 V), which would then act as the cathode and accelerate the corrosion of aluminum matrix[22]. Therefore, the pitting holes on the surface of all immersed alloy wires appeared in the form of islands. However, the shape and distribution of FeAl_3 phase particles varied during the cold drawing process, wherein the equiaxial grains in the alloys were elongated to fibrous grains along the drawing direction on I section, and the large size grains were pressed into small size grains on II section. Thus, the density of grain boundaries and the amount of grains increased in the unit area of the alloys with the increasing cold drawing strain. In contrast, the large size FeAl_3 phase particles were elongated and fragmented into small size particles on I section, while the large size FeAl_3 phase particles on II section were pressed into small globular particles. As such, in the unit area of the alloys, as the cold drawing strain increased, the amount of the second phase particles increased and its size decreased. However, the amount of the second phase particles was a constant on the entire II section during the cold drawing process.

The introduction of dislocations and grain boundaries by plastic strain will cause the corrosion resistance of the alloys to deteriorate[23]. However, compact structure can be obtained by plastic deformation, which is beneficial to the improvement of corrosion resistance. As a result, the corrosion resistance of metals can be not monotonically degraded or enhanced by the grain size, dislocation and grain boundary density[23-25]. The finding in our study showed that, the E_{corr} on both I and II sections increased first and then decreased with the increasing cold drawing strain, supporting that the corrosion sensibility of the Al-3.0 wt.%Mg alloy should decrease first and then increase during the cold drawing process. Additionally, the combination of dislocations, grain boundaries, grain size and structural

compaction affected the evolution of corrosion sensibility and E_{corr} . However, the decrease of i_{corr} and the increase of E_{pit} along with the increasing strain indicated that the corrosion resistance increased and pitting sensibility decreased during the cold drawing process.

Pitting occurred around $FeAl_3$ phase particles. The more and the larger the second phases, the more and the larger the pitting holes. During the cold drawing process, $FeAl_3$ phase particles were elongated on I section and pressed on II section. In particular, the number of $FeAl_3$ phase particles increased per unit area in both I and II sections, and the particles size decreased with the increasing strain, which could result in the improvement of corrosion resistance and the reduction of pitting sensibility. Therefore, as the cold drawing strain increased, the i_{corr} decreased, E_{pit} and capacitive circle diameter of the Al-3.0 wt.%Mg alloy wire increased on both I and II sections.

In this study, the E_{pit} , R_t and $R_{t(pit)}$ of the alloy wires on I section were lower and smaller than those on II section with the same strain, and the i_{corr} on I section was higher than that on II section, demonstrating that the cold-drawn Al-3.0 wt.%Mg alloy on cross section (II section) had better corrosion resistance and lower pitting sensibility compared to the alloy on longitudinal section (I section) with the same cold drawing strain. This could be due to the microstructure and second phases evolution during the cold drawing process. It is known that compression can achieve a more compact structure compared to stretching. Therefore, the structure of the alloy on II section was more compact than that on I section. In addition, our result showed that one $FeAl_3$ phase particle was elongated and fragmented to several particles on I section, while one $FeAl_3$ phase particle was just pressed to smaller ones on II section. It is believed that the more compact, less and smaller $FeAl_3$ phase particles helped obtain better corrosion resistance and lower pitting sensibility on II section. Finally, the difference of microstructure, amount and size of $FeAl_3$ phase particles between I and II sections became greater with the increasing cold drawing strain, which could result in the increase of $i_{corr-II} - i_{corr-I}$ value and $E_{pit-II} - E_{pit-I}$ value.

4. CONCLUSION

(1) During the cold drawing process, the equiaxial grains of Al-3.0 wt.%Mg alloy were elongated to fibrous grains on I section, while the grains with large size were pressed to small size grains on II section. Moreover, the large size skeletal $FeAl_3$ phase particles were elongated and fragmented to small size lining particles on I section, while the large size particles on II section were pressed to small globular particles.

(2) With the increasing cold drawing strain, the corrosion resistance of Al-3.0 wt.%Mg alloy increased and the pitting sensibility decreased, while the corrosion sensibility increased first and then decreased.

(3) Compared to the alloy on I section, the alloy on II section had better corrosion resistance and lower pitting sensibility. The difference of corrosion resistance and pitting sensibility between I and II sections increased with the increasing strain.

ACKNOWLEDGEMENTS

This study was financially supported by “Nantong Municipal Science and Technology Project (JC2018047), the Fundamental Research Funds for the Central Universities (2018B02514), National Science Foundation of China (51909071) and Natural Science Foundation of Jiangsu Province (BK20190493)”.

References

1. Z.G. Wu, M. Song and Y.H. He, *Mater. Sci. Eng., A*, 504 (2009) 183.
2. H.H. Chen, J.Y. Wang, J. Lee and S. Lee, *J. Alloys Compd.*, 460 (2008) 305.
3. M.M. Sharma and C.W. Ziemian, *J. Mater. Eng. Perform.*, 17 (2008) 870.
4. P. Kustra, A. Milenin, D. Byrska-Wójcik, O. Grydin and M. Schaper, *J. Mater. Process. Technol.*, 247 (2017) 234.
5. T.S. Cao, C. Vachey, P. Montmitinnet and P.O. Bouchard, *J. Mater. Process. Technol.*, 217 (2015) 30.
6. K. Hanazaki, N. Shigeiri and N. Tsuji, *Mater. Sci. Eng., A*, 527 (2010) 5699.
7. A. Korchef and A. Kahoul, *Int. J. Corros.*, 2013 (2013) 1.
8. E. Akiyama, Z.G. Zhang, Y. Watanabe and K. Tsuzaki, *J. Solid State Electrochem.*, 13 (2009) 277.
9. J.G. Brunner, N. Birbilis, K.D. Ralston and Sahalia Celene Virtanen, *Corros. Sci.*, 57 (2012) 209.
10. T. Chen, H. John, J. Xu, Q.H. Lu, J. Hawk and X.B. Liu, *Corros. Sci.*, 77 (2013) 230.
11. N.C. Renton, A.M. Elhoud and W.F. Deans, *J. Mater. Eng. Perform.*, 20 (2011) 436.
12. G. Ben Hamu, D. Eliezer and L. Wagner, *J. Alloys Compd.*, 468 (2009) 222.
13. H. Krawiec, V. Vignal, J. Loch and P. Erazmus-Vignal, *Corros. Sci.*, 96 (2015) 160.
14. W.Y. Guo, J. Sun and J.S. Wu, *Mater. Charact.*, 60 (2009) 173.
15. X. Zhang, Z.H. Wang, Z.H. Zhou and J. Shao, *Appl. Phys. A*, 124 (2018) 691.
16. G3-13, Annual Book of ASTM Standards, Standard Practice for Conventions Applicable to Electrochemical Measurement in Corrosion Testing, ASTM, 2013.
17. X. Zhang, Z.H. Wang, Z.H. Zhou and J.M. Xu, *J. Wuhan Univ. Technol.*, 32 (2017) 611.
18. X. Zhang, Z.H. Wang, Z.H. Zhou and Jianming Xu, *J. Mater. Eng. Perform.*, 25 (2016) 1122.
19. Y.J. Shi, Q.L. Pan, M.J. Li, X. Huang and B. Li, *J. Alloys Compd.*, 612 (2014) 42.
20. X. Zhang, Z.H. Wang, Z.H. Zhou and J.M. Xu, *J. Alloys Compd.*, 698 (2017) 241.
21. T.J. Luo, Y.S. Yang, Y.J. Li and X.G. Dong, *Electrochim. Acta*, 54 (2009) 6433.
22. Z.H. Huang, X.F. Guo, Z.M. Zhang and C.J. Xu, *Acta Metall. Sinica*, 18 (2005) 129.
23. S.G. Wang, Y.J. Huang, H.B. Han, M. Sun, K. Long and Z.D. Zhang, *J. Electroanal. Chem.*, 725 (2014) 95.
24. Y. Li, F.H. Wang and G. Liu, *Corrosion*, 60 (2004) 891.
25. X.Y. Wang and D.Y. Li, *Electrochim. Acta*, 47 (2002) 3939.